

AD-A054 372 ARMY ARMAMENT RESEARCH AND DEVELOPMENT COMMAND ABERD--ETC F/G 14/2
PROPOSED DESIGN FOR A DIFFERENTIAL PRESSURE GAGE TO MEASURE DYN--ETC(U)
MAR 78 N H ETHRIDGE

UNCLASSIFIED

ARBRL-MR-02814

SBIE-AD-E430 012

NL

1 OF 1
AD
A054372



BRL



END
DATE
FILMED
6 -78
DDC

FOR FURTHER TRAN

12

4/28

AD-E430 012

AD

AD A 054372

ARBRL-MR-02814

BRL

MEMORANDUM REPORT ARBRL-MR-02814

PROPOSED DESIGN FOR A DIFFERENTIAL
PRESSURE GAGE TO MEASURE DYNAMIC
PRESSURE IN BLAST WAVES

Noel H. Ethridge

March 1978

Approved for public release; distribution unlimited.

DDC
RECEIVED
MAY 31 1978
B

USA ARMAMENT RESEARCH AND DEVELOPMENT COMMAND
USA BALLISTIC RESEARCH LABORATORY
ABERDEEN PROVING GROUND, MARYLAND

AD No. JDC FILE COPY

Destroy this report when it is no longer needed.
Do not return it to the originator.

Secondary distribution of this report by originating
or sponsoring activity is prohibited.

Additional copies of this report may be obtained
from the National Technical Information Service,
U.S. Department of Commerce, Springfield, Virginia
22161.

The findings in this report are not to be construed as
an official Department of the Army position, unless
so designated by other authorized documents.

*The use of trade names or manufacturers' names in this report
does not constitute indorsement of any commercial product.*

(18) SBIE

(19) AD-E430 012

UNCLASSIFIED

SECURITY CLASSIFICATION OF THIS PAGE (When Data Entered)

REPORT DOCUMENTATION PAGE		READ INSTRUCTIONS BEFORE COMPLETING FORM
1. REPORT NUMBER MEMORANDUM REPORT ARBRL-MR-02814	2. GOVT ACCESSION NO.	3. RECIPIENT'S CATALOG NUMBER
4. TITLE (and Subtitle) PROPOSED DESIGN FOR A DIFFERENTIAL PRESSURE GAGE TO MEASURE DYNAMIC PRESSURE IN BLAST WAVES.	5. TYPE OF REPORT & PERIOD COVERED Final Repts.	6. PERFORMING ORG. REPORT NUMBER
7. AUTHOR(s) Noel H. Ethridge	8. CONTRACT OR GRANT NUMBER(s)	9. PROGRAM ELEMENT, PROJECT, TASK AREA & WORK UNIT NUMBERS RDT&E J11AAXS(352)
10. PERFORMING ORGANIZATION NAME AND ADDRESS US Army Ballistic Research Laboratory (ATTN: DRDAR-BLT) Aberdeen Proving Ground, MD 21005	11. REPORT DATE MAR 1978	12. NUMBER OF PAGES 41
13. CONTROLLING OFFICE NAME AND ADDRESS US Army Armament Research & Development Command US Army Ballistic Research Laboratory (ATTN: DRDAR-BL) Aberdeen Proving Ground, MD 21005	14. MONITORING AGENCY NAME & ADDRESS (if different from Controlling Office) Defense Nuclear Agency Washington, D.C. 20305	15. SECURITY CLASS. (of this report) UNCLASSIFIED
16. DISTRIBUTION STATEMENT (of this Report) Approved for public release; distribution unlimited.		
17. DISTRIBUTION STATEMENT (of the abstract entered in Block 20, if different from Report)		
18. SUPPLEMENTARY NOTES		
19. KEY WORDS (Continue on reverse side if necessary and identify by block number) Dynamic Pressure Gage Pressure Gage Diaphragms Dynamic Pressure Measurements Shock Tube Instrumentation Pressure Gage Blast Gage Blast Wave Measurements Air Flow Gage		
20. ABSTRACT (Continue on reverse side if necessary and identify by block number) (mba) The current technique for determining dynamic pressure in blast waves is subject to large errors below incident shock over pressures of 69 kPa (10 psi). It is shown that if a single pressure-sensing element can be used to measure the differential pressure between stagnation and side-on overpressures, then dynamic pressure can be determined with much less error. A design for a differential pressure gage is presented. A particular diaphragm size and material are proposed, and several diaphragm deflection-sensing techniques are indicated. The frequency response of the gage seems adequate for measurements.		

DD FORM 1 JAN 73 1473

EDITION OF 1 NOV 65 IS OBSOLETE

UNCLASSIFIED

(Continued)

SECURITY CLASSIFICATION OF THIS PAGE (When Data Entered)

393 474

next page

UNCLASSIFIED

SECURITY CLASSIFICATION OF THIS PAGE(When Data Entered)

(Item 20 Continued)

of blast waves from large HE charges.

UNCLASSIFIED

SECURITY CLASSIFICATION OF THIS PAGE(When Data Entered)

TABLE OF CONTENTS

	Page
LIST OF ILLUSTRATIONS	5
I. INTRODUCTION	7
II. CURRENT TECHNIQUE FOR DETERMINING DYNAMIC PRESSURE	7
III. PROPOSED TECHNIQUE FOR DETERMINING DYNAMIC PRESSURE	10
IV. PROPOSED GAGE DESIGN	12
V. SUMMARY	25
ACKNOWLEDGEMENT	25
LIST OF SYMBOLS	27
DISTRIBUTION LIST	29

ACCESSION for		
NTIS	White Section	<input checked="" type="checkbox"/>
DDC	Buff Section	<input type="checkbox"/>
UNANNOUNCED		<input type="checkbox"/>
JUSTIFICATION _____		
BY _____		
DISTRIBUTION/AVAILABILITY CODES		
Dist.	AVAIL	and/or SPECIAL
A		

LIST OF ILLUSTRATIONS

Figure		Page
1.	Maximum and minimum percent error in dynamic pressure versus shock front overpressure calculated using Equation 4 and the assumption of plus or minus three percent error in P_T and P_S	11
2.	Ratio of dynamic pressure P_q to differential pressure D_q versus incident shock overpressure P_S . The dashed curves show the change produced by increasing or decreasing P_S used in Equation 9 by the factors 1.5 or 0.5, respectively	13
3.	Proposed Design for a Differential Pressure Gage	15
4.	Variation of stagnation pressure indication with angle of attack and geometry for Pitot tubes, from Reference 6	17
5.	Nose and stem effects on side-on overpressure measurements along a static pressure tube, from Reference 6	18
6.	Effect of Orifice Edge Form on Side-on Pressure Measurement, from Reference 6	19
7.	Graphical solution for the fundamental frequency of any clamped, circular, flat diaphragm under radial tension, from Reference 2	24

I. INTRODUCTION

The loading on a target produced by the blast wave from a large-scale explosion is usually described in terms of two phases. The diffraction phase occurs first and involves the phenomena produced when the shock front encounters and engulfs the target. The drag phase occurs after the rapid pressure variations associated with the diffraction process have ceased and a quasi-steady flow has been established over the target. The loading due to one or both phases may produce damage to the target, and therefore must be defined for calculating the response of the target or for correlating the response with previous test results.

On field experiments where targets are exposed to long-duration blast waves, overpressure as a function of time at the target or on the target can be recorded for use in determining the diffraction phase loading. Measurement of overpressure-time profiles at pressure levels of interest for military equipment can be performed satisfactorily using presently available instrumentation.

For determining drag phase loading on the target, the dynamic pressure is required as a function of time at the target location. The dynamic pressure is generated by the air flow occurring in the blast wave. Dynamic pressure currently is derived from separate measurements of stagnation overpressure and side-on overpressure versus time. Large errors in the determination of dynamic pressure may occur using the current technique at shock front overpressures less than 69 kPa (10 psi). Many critical items of Army equipment, such as communication systems, are damaged at incident blast overpressure levels less than 69 kPa (10 psi). The capability for making accurate measurements of dynamic pressure in the range of shock front overpressures as low as 21 kPa (3 psi) is required.

The purpose of this report is to present a design for a gage which offers the possibility of determining dynamic pressure versus time with satisfactory accuracy at such low incident blast overpressures.

II. CURRENT TECHNIQUE FOR DETERMINING DYNAMIC PRESSURE

The current technique for the determination of dynamic pressure in a blast wave involves the use of independent measurements of stagnation overpressure and side-on overpressure from gages which are physically separated, usually by several feet. The records from these gages are used to compute the dynamic pressure by use of fluid flow relations which are described, for example, in Reference 1. For this report only the subsonic flow regime is of interest, and the computational technique is described below.

¹H. W. Liepmann and A. Roshko, "Elements of Gasdynamics," John Wiley and Sons, Inc., New York, New York, 1957, p. 148-149. For derivation of dynamic pressure at a shock front, use equations on page 64.

It is assumed that the fluid at the point of measurement experiences only isentropic changes. Then:

$$P_T = (P_S + P_A) [1 + (\gamma - 1)M^2/2]^{\gamma/(\gamma - 1)} - P_A \quad (1)$$

where:

P_T = stagnation overpressure

P_S = side-on overpressure

P_A = ambient atmospheric pressure

γ = ratio of specific heats (assumed to be 1.4)

M = flow Mach number.

P_T and P_S are the quantities recorded by the stagnation and side-on overpressure gages used in field experiments.

Equation 1 is rearranged to provide M^2 :

$$M^2 = [2/(\gamma - 1)] \left\{ [(P_T + P_A)/(P_S + P_A)]^{(\gamma - 1)/\gamma} - 1 \right\}. \quad (2)$$

The dynamic pressure P_q is obtained from the overpressure value and the flow Mach number:

$$P_q = (\gamma/2) (P_S + P_A) M^2 \quad (3)$$

where:

P_q = dynamic pressure = $1/2 \rho u^2$

ρ = density

u = particle velocity.

When the value of M^2 from Equation 2 is substituted into Equation 3, dynamic pressure P_q can be expressed in terms of P_T and P_S :

$$P_q = [\gamma/(\gamma - 1)] (P_S + P_A) \left\{ [(P_T + P_A)/(P_S + P_A)]^{(\gamma - 1)/\gamma} - 1 \right\}. \quad (4)$$

The current technique for determining dynamic pressure in the subsonic flow regime is to insert the independently derived values of P_T and P_s into Equation 4 and calculate P_q .

At the blast wave shock front¹:

$$P_q = P_s^2 / [(\gamma - 1)P_s + 2\gamma P_A] = 2.5 P_s^2 / (P_s + 7P_A) \text{ for } \gamma = 1.4 \quad (5)$$

where the value of P_s is that for the incident peak overpressure.

If Equation 3 is solved for M^2 in terms of P_q and the result substituted into Equation 1, then:

$$P_T = (P_s + P_A) \left[1 + \frac{\gamma - 1}{\gamma} \frac{P_q}{(P_s + P_A)} \right]^{\frac{\gamma}{\gamma - 1}} - P_A \quad (6)$$

Using the value of P_q given by Equation 5 and $\gamma = 1.4$ in Equation 6, the value of P_T for shock front conditions is found to be:

$$P_T = (P_s + P_A) \left[1 + \frac{5}{7} \frac{P_s^2}{(P_s + P_A)(P_s + 7P_A)} \right]^{7/2} - P_A \quad (7)$$

For a given predicted incident shock front overpressure P_s , Equation 7 provides the corresponding value of P_T .

To obtain an indication of the error possible in P_q calculated using Equation 4 and independently measured values of P_T and P_s , calculations were made for P_q under the assumption that the values of P_T and P_s had a maximum error of three percent. The particular values of P_T and P_s used were for shock front conditions, so that for a given incident shock overpressure P_s the corresponding value of P_T was calculated from Equation 7. The values of P_T and P_s were multiplied by the factors 1.03 and 0.97 and substituted into Equation 4. The maximum value of P_q was obtained for the combination of P_T three percent high and P_s three percent low, while the minimum value for P_q was obtained for P_T three percent low and P_s three percent high.

The percent error e in P_q was calculated as follows:

$$e = \frac{P'_q - P_q}{P_q} \times 100 \quad (8)$$

where:

$P'_q = P_q$ calculated from Equation 4 using values of P_T and P_s , multiplied by 1.03 or 0.97 as indicated above.

$P_q =$ value of P_q at shock front with peak overpressure of P_s , as calculated using Equation 5.

The results for c using the maximum three percent error in the values of P_T and P_s are shown in Figure 1. The value of P_A used was 101.325 kPa (14.696 psi).

Below about 100 kPa (14.5 psi) the error increases rapidly. At 69 kPa (10 psi) it is ± 28 percent, at 34.5 kPa (5 psi) it is ± 54 percent, and at 21 kPa (3 psi) the value is ± 87 percent. These values represent the error possible in determining the peak dynamic pressure assuming a maximum error of plus or minus three percent error in the measured values of P_T and P_s . In determining the dynamic pressure-time profile, the error will increase behind the shockfront as the values of P_T and P_s decrease.

It is questionable whether the present instrumentation systems can provide pressure measurements in the field which have no more than three percent error, and it seems unlikely that a significant reduction below three percent can be achieved. Thus the current technique of determining dynamic pressure by using separate measurements of P_T and P_s is unsatisfactory for the lower overpressure levels of interest.

III. PROPOSED TECHNIQUE FOR DETERMINING DYNAMIC PRESSURE

The difficulty in the current technique of using independent measurements of stagnation overpressure and side-on overpressure to determine dynamic pressure is that at low side-on overpressures the errors in the measured signals may become as large or larger than the magnitude of the dynamic pressure. Thus the value of the differential pressure ($P_T - P_s$) calculated from independently measured values of P_T and P_s may be very much in error. However, if a sensing element can be used which will measure this differential pressure directly with no more error than occurs in the usual field pressure measurement, then dynamic pressure can be determined to about the same level of accuracy. At low overpressures this differential pressure is essentially equal to the dynamic pressure.

If Equation 4 is rearranged to express P_q in terms of the differential pressure D_q and P_s , the result is:

$$P_q = [\gamma/(\gamma - 1)](P_s + P_A) \left\{ [1 + D_q/(P_s + P_A)]^{(\gamma - 1)/\gamma} - 1 \right\} \quad (9)$$

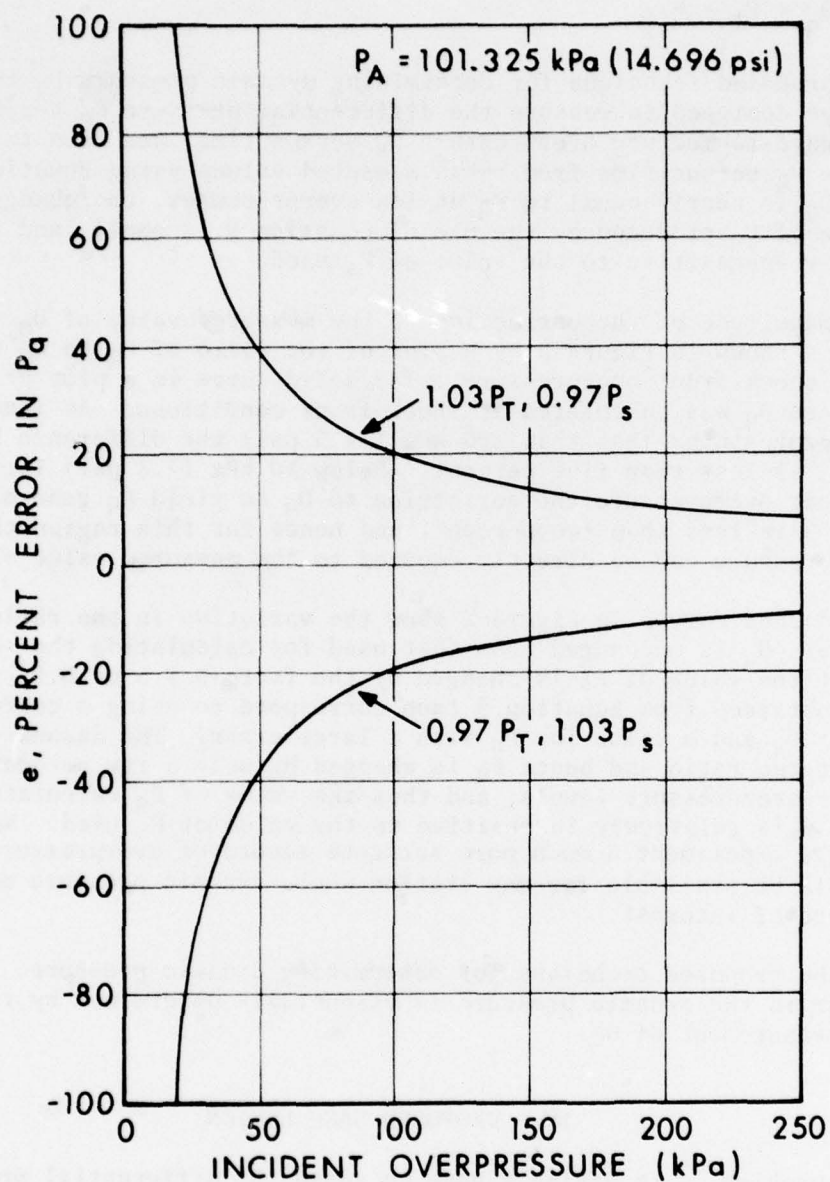


Figure 1 Maximum and minimum percent error in dynamic pressure versus shock front overpressure calculated using Equation 4 and the assumption of plus or minus three percent error in P_T and P_s .

where: $D_q = P_T - P_S$.

The proposed technique for determining dynamic pressure P_q is to use a gage designed to measure the differential pressure D_q versus time, another gage to measure overpressure P_S versus time, and then to calculate P_q versus time from these measured values using Equation 9. Because D_q is nearly equal to P_q at low overpressures, the change from the value of D_q produced by the use of Equation 9 is small, and is relatively insensitive to the value of P_S used.

The magnitude of the correction to the measured value of D_q to provide P_q is shown in Figure 2 by a plot of the ratio of P_q to D_q versus incident shock front overpressure. The solid curve is a plot of the ratio where D_q was calculated at shock front conditions. At incident shock overpressures less than 100 kPa (14.5 psi) the difference between P_q and D_q is less than five percent. Below 50 kPa (7.3 psi) incident shock front overpressure the correction to D_q to yield P_q generated by Equation 9 is less than two percent, and hence for this region the dynamic pressure can be directly equated to the measured value of D_q .

The dashed curves in Figure 2 show the variation in the ratio of P_q to D_q where D_q is unchanged from that used for calculating the solid curve but the value of P_S is changed by the factors 1.5 or 0.5. The results obtained from Equation 9 then correspond to using a correct value for D_q and a value for P_S with a large error. The dashed curves show that the ratio and hence P_q is changed by only a few percent at the lower overpressure levels, and thus the value of P_q calculated from Equation 9 is relatively insensitive to the value of P_S used. Normally on a field experiment a much more accurate record of overpressure versus time would be available for any station where dynamic pressure measurements were of interest.

In the proposed technique for determining dynamic pressure, then, the error in the dynamic pressure is essentially determined by the error in the measurement of D_q .

IV. PROPOSED GAGE DESIGN

The problem is to devise a gage to sense the differential pressure $P_T - P_S$ with reasonable accuracy (about five percent error) and adequate frequency response (zero to several thousand Hertz) suitable for use for measurements on HE blast experiments. The pressure-sensing element must respond to low differential pressures and yet have the required range of frequency response. The housing for the sensing element must minimize errors in pressure developed at pressure input ports. The entire gage must be as small as possible to minimize loss in frequency response due to long path lengths between pressure input ports and

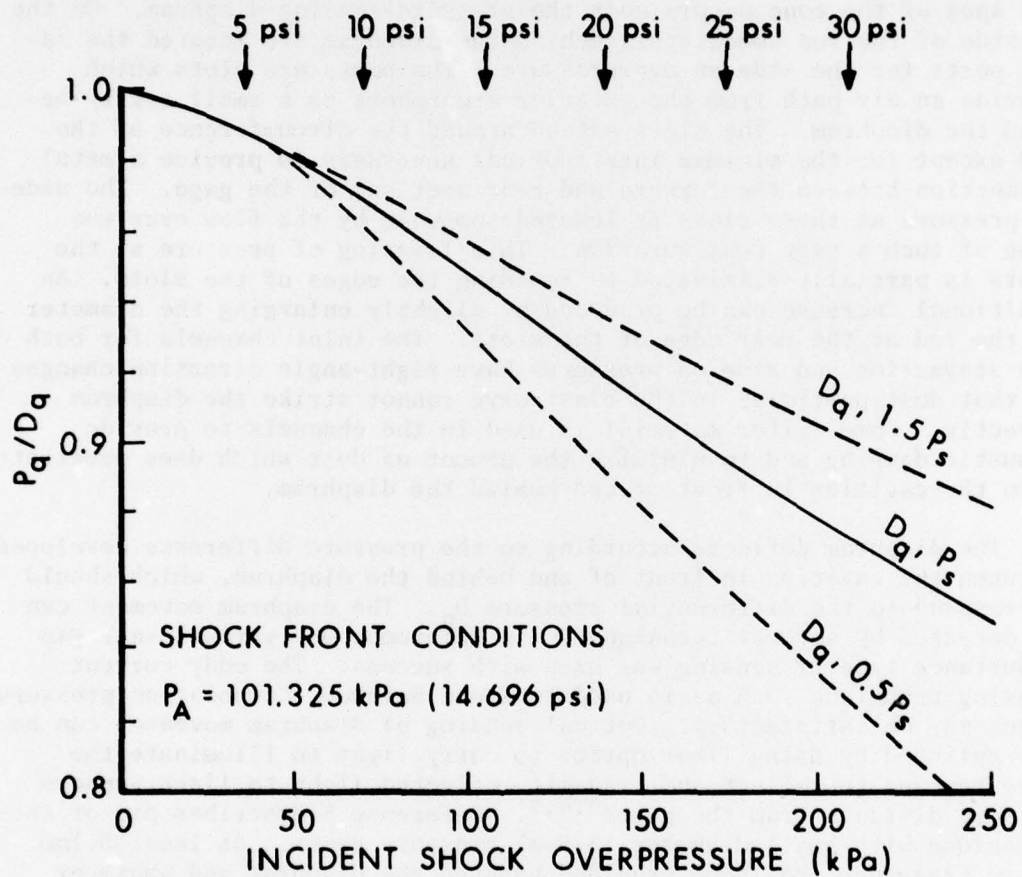


Figure 2 Ratio of dynamic pressure P_q to differential pressure D_q versus incident shock overpressure P_s . The dashed curves show the change produced by increasing or decreasing P_s used in Equation 9 by the factors 1.5 or 0.5, respectively.

the sensing element.

A proposed design for a differential pressure gage is shown in Figure 3. The outer configuration is that of a long cylindrical rod which is oriented parallel to the expected direction of air flow. The input pressure port for the stagnation overpressure is located in the nose of the rod, and is in the shape of a 15 degree half-angle cone. The apex of the cone occurs near the pressure-sensing diaphragm. On the outside of the rod immediately behind the diaphragm are located the input ports for the side-on overpressure. The ports are slots which provide an air path from the exterior atmosphere to a small cavity behind the diaphragm. The slots extend around the circumference of the rod except for the minimum interruptions necessary to provide a metal connection between the forward and rear sections of the gage. The side-on pressure at these slots is lowered somewhat by the flow over the nose of such a gage configuration. This lowering of pressure at the slots is partially eliminated by rounding the edges of the slots. An additional increase can be produced by slightly enlarging the diameter of the rod at the rear edge of the slots. The inlet channels for both the stagnation and side-on pressures have right-angle direction changes so that dust particles in the blast wave cannot strike the diaphragm directly. Some filter material is used in the channels to provide acoustic damping and to minimize the amount of dust which does penetrate into the cavities in front of and behind the diaphragm.

The diaphragm deflects according to the pressure difference developed between the cavities in front of and behind the diaphragm, which should correspond to the differential pressure D_q . The diaphragm movement can be detected by several techniques. In Reference 2 a variable-air-gap inductance type of sensing was used with success. The eddy current sensing technique such as is used in Kaman Sciences Corporation pressure gages may be satisfactory. Optical sensing of diaphragm movement can be accomplished by using fiber optics to carry light to illuminate the diaphragm and to collect and transmit reflected light to light sensors at some distance from the gages^{3,4,5}. Reference 5 describes use of this technique with small-diameter (3-5mm) pressure gages. At least 0.1mm or so clearance should be provided between the diaphragm and whatever

²John L. Patterson, "A Miniature Electrical Pressure Gage Utilizing a Stretched Flat Diaphragm," NACA Technical Note 2659, 1952.

³R. Bailly-Salins, "Plastic Optical Fiber Displacement Sensor for Study of the Dynamic Response of a Solid Exposed to an Intense Pulsed Electron Beam," *Rev. Sci. Instrum.*, Volume 46, No. 7, July 1975.

⁴J. Anthony Powell, "A Simple Two-Fiber Optical Displacement Sensor," *Rev. Sci. Instrum.*, Volume 45, No. 2, February 1974.

⁵Gordon W. Margerum et al., "Fiber Optic and Laser Digital Pressure Transducers," *Progress in Astronautics and Aeronautics*, Volume 34, Instrumentation for Airbreathing Propulsion, 1974.

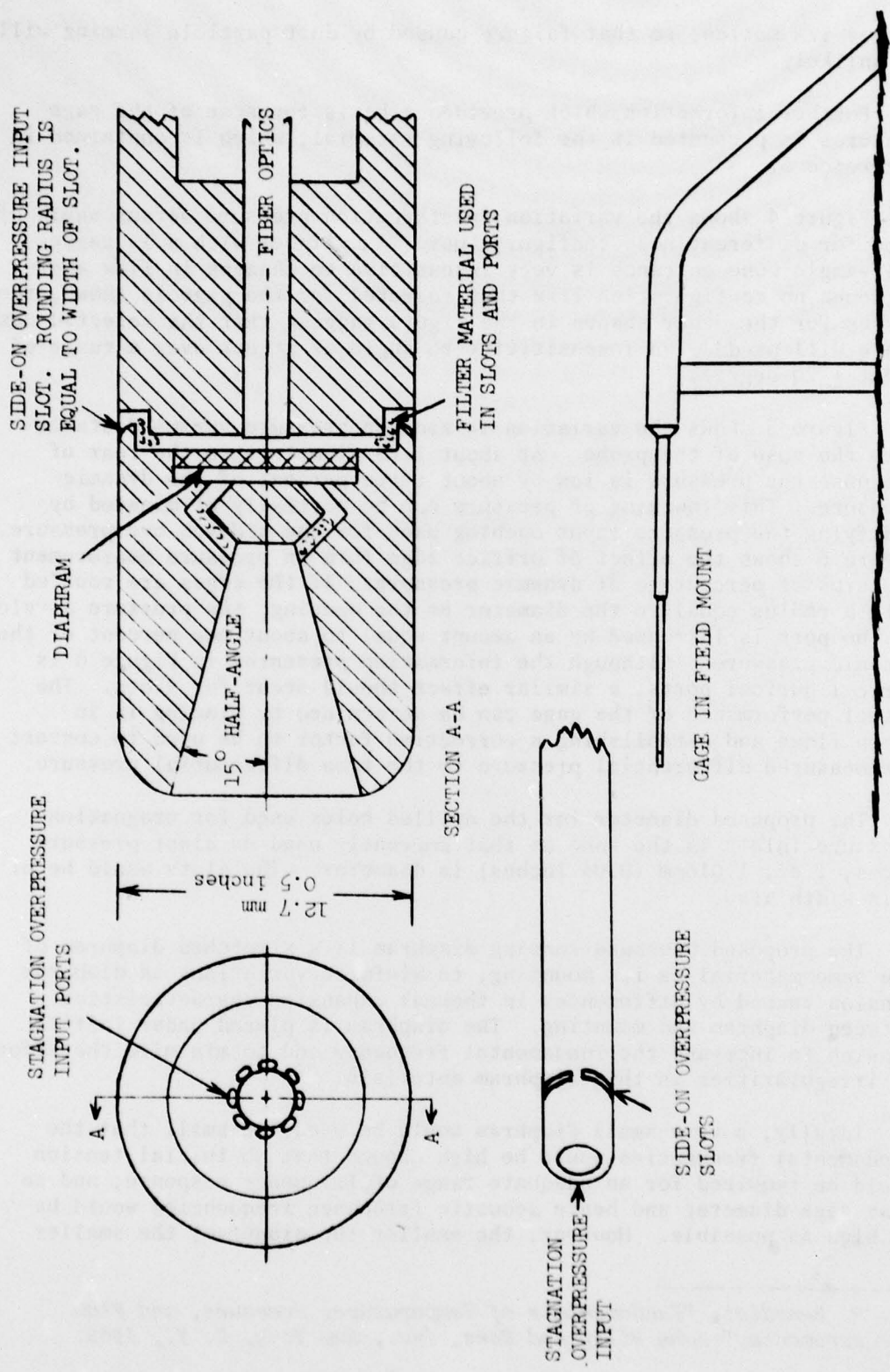


Figure 3 Proposed differential pressure gage design.

senses its motion, so that failure caused by dust particle jamming will be unlikely.

Further information which provided a basis for some of the gage features is presented in the following material, which is contained in Reference 6.

Figure 4 shows the variation in stagnation pressure versus angle of flow for different nose configurations. A cylinder with a 15 degree half-angle cone entrance is very insensitive to changes in flow angle. Although no configuration like that selected for the gage is shown, the curves for the other shapes in the figure suggest that the selected nose shape will produce an insensitivity to angle of attack over a range of about ± 20 degrees.

Figure 5 shows the variation in side-on pressure versus distance from the nose of the probe. At about 1.25 diameters to the rear of the nose the pressure is low by about three percent of the dynamic pressure. This lowering of pressure can be partially eliminated by modifying the pressure input opening used for the side-on overpressure. Figure 6 shows the effect of orifice edge form on pressure measurement in terms of percentage of dynamic pressure. If the edges are rounded with a radius equal to the diameter of the opening, the pressure developed in the port is increased by an amount equal to about one percent of the dynamic pressure. Although the information presented in Figure 6 is for cylindrical ports, a similar effect should occur for slots. The actual performance of the gage can be determined by placing it in known flows and establishing a correction factor to be used to convert the measured differential pressure to the true differential pressure.

The proposed diameter for the drilled holes used for stagnation pressure inlets is the same as that currently used on blast pressure gages, i.e., 1.016mm (0.04 inches) in diameter. The slots would be of this width also.

The proposed pressure-sensing diaphragm is a stretched diaphragm of the same material as its mounting, to minimize variations in diaphragm tension caused by differences in thermal expansion characteristics between diaphragm and mounting. The diaphragm is placed under initial tension to increase the fundamental frequency and to minimize the effects of irregularities in thin diaphragm materials.

Ideally, a very small diaphragm would be used, so small that the fundamental frequencies would be high enough that no initial tension would be required for an adequate range of frequency response, and so that gage diameter and hence acoustic resonance frequencies would be as high as possible. However, the smaller the diaphragm, the smaller

⁶ R. P. Benedict, "Fundamentals of Temperature, Pressure, and Flow Measurements," John Wiley and Sons, Inc., New York, N. Y., 1969.

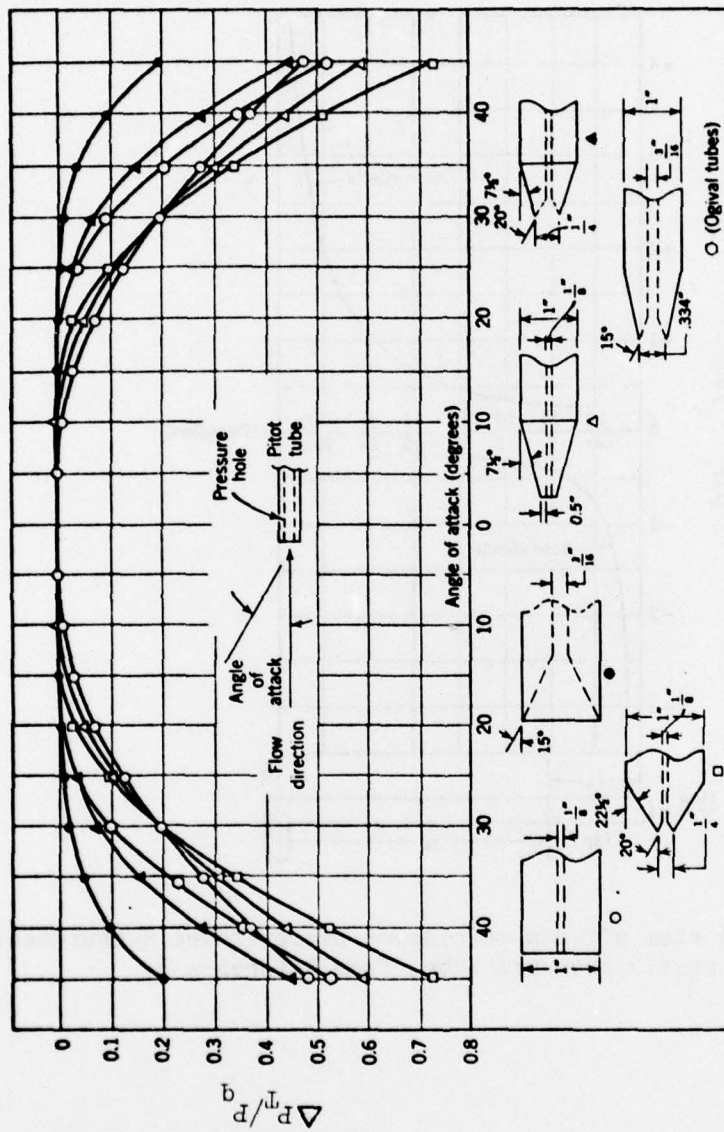


Figure 4 Variation of stagnation pressure indication with angle of attack and geometry for Pitot tubes, from Reference 6.

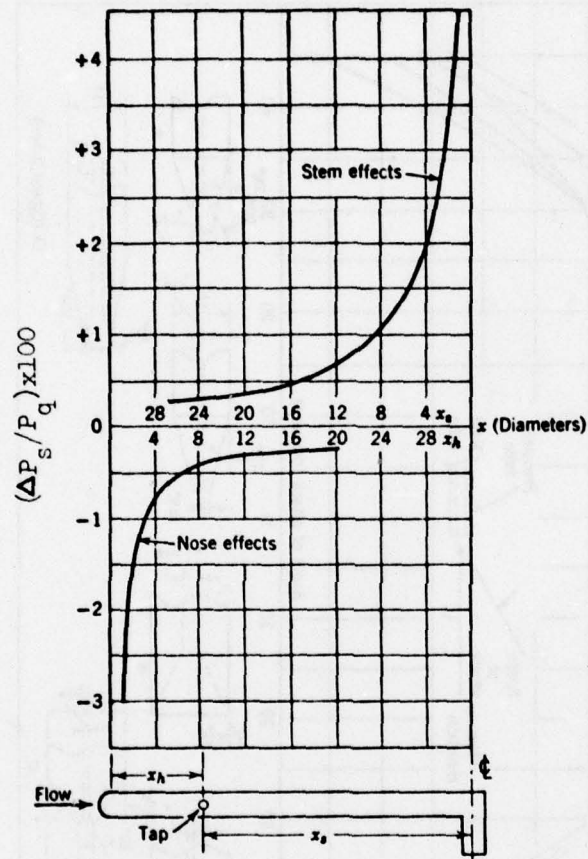


Figure 5 Nose and stem effects on side-on overpressure measurements along a static pressure tube, from Reference 6.

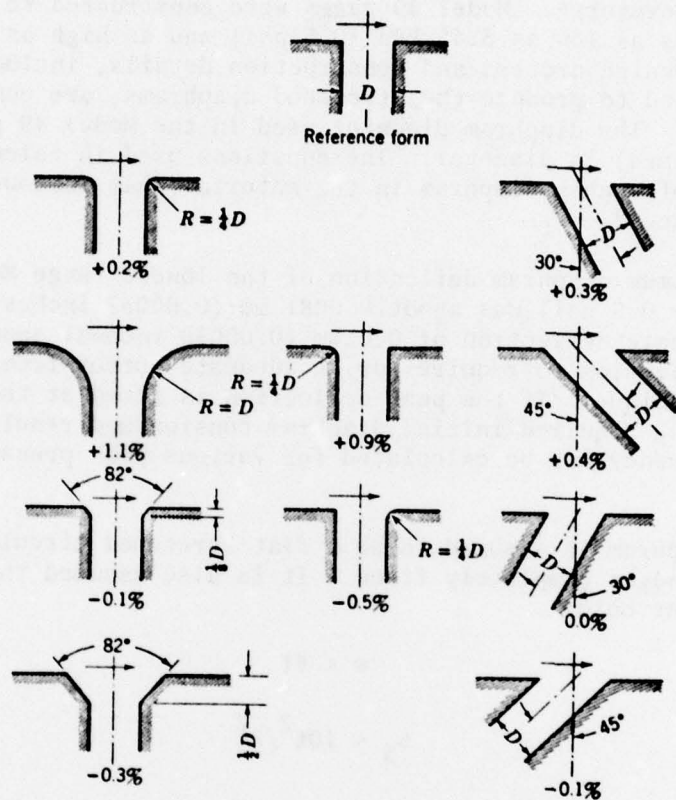


Figure 6 Effect of orifice edge form on side-on pressure measurement, from Reference 6. The variation is listed in percentage of dynamic pressure.

the deflection to be sensed, and hence obtaining a useful signal from the gage becomes more difficult.

An initial proposed diaphragm is of a nickel-iron alloy that was successfully used in the NACA miniature electrical pressure gage Model 49, designed by the Instrument Research Division of the Langley Aeronautical Laboratory². Model 49 gages were constructed to measure maximum pressures as low as 3.45 kPa (0.5 psi) and as high as 689 kPa (100 psi). The design process and construction details, including the technique used to produce the stretched diaphragms, are contained in Reference 2. The diaphragm diameter used in the Model 49 gage was 7.94 mm (5/16 inches) in diameter. The equations used in calculating the properties of such a diaphragm in the material that follows were taken from Reference 2.

The maximum diaphragm deflection of the lowest range Model 49 gage (3.45 kPa or 0.5 psi) was about 0.0081 mm (0.00032 inches). Thus a peak full scale deflection of 0.01mm (0.00039 inches) seems a reasonable minimum deflection to require for an adequate output from a deflection-sensing technique. If the peak deflection is fixed at this value, the corresponding required initial diaphragm tension and resulting fundamental frequency can be calculated for various peak pressures of interest.

The diaphragm is assumed to be a flat stretched circular diaphragm having its edges completely fixed. It is also assumed that the following relations hold:

$$w < 8t$$

$$s_o < 10t^2/R^2$$

where:

w = deflection of diaphragm at center

t = diaphragm thickness

R = diaphragm radius

s_o = strain due to initial diaphragm tension.

Then:

$$D_q = \frac{16}{3} \frac{E t^3 w}{(1 - \sigma^2) R^4} \left[1 + \frac{5(1 + \sigma)}{6} s_o \frac{R^2}{t^2} + \frac{(1 + \sigma)(173 - 73\sigma)}{360} \frac{w^2}{t^2} \right] \quad (10)$$

where:

D_q = differential pressure

E = Young's Modulus of elasticity

σ = Poisson's ratio.

A range of differential pressures corresponding to incident side-on overpressures were calculated. For these pressures and the diaphragm thicknesses listed in Reference 2 and for a peak deflection of 0.01 mm, the initial strains s_o were calculated by solving Equation 10 for s_o as follows:

$$s_o = \frac{9(1 - \sigma)R^2}{40 E w t} D_q - \frac{6t^2}{5(1 + \sigma)R^2} - \frac{(173-73\sigma)w^2}{300 R^2} . \quad (11)$$

The values obtained for s_o are shown in Table I, where the parameter values used were as follows:

$R = 3.969 \text{ mm (5/32 inches)}$

$E = 1.517 \times 10^8 \text{ kPa (22 x } 10^6 \text{ psi)}$ for 42 percent nickel and 58 percent iron alloy

$\sigma = 0.29$

$w = 0.01\text{mm (0.0003937 inches)}$.

The non-linearity of the deflection versus pressure curve is indicated by the ratio R_N of the last term in the brackets of Equation 10 to the other terms in the bracket:

$$R_N = \frac{(1 + \sigma)(173 - 73\sigma) w^2}{360 t^2 + 300(1 + \sigma) s_o R^2} . \quad (12)$$

The percent non-linearity, then, is:

$$P_N = 100 R_N \quad (13)$$

The percent non-linearity calculated for pressures of interest is listed in Table I also.

A graphical solution for the fundamental frequencies of a stretched diaphragm is contained in Reference 2. The result is utilized below.

Table I. Diaphragm Properties for Various Peak Overpressures for a Peak Deflection of 0.01 mm (0.0003937 inches)

P_s (kPa)	P_s (psi)	P_T (kPa)	P_T (psi)	P_q (kPa)	P_q (psi)	D_q (kPa)	D_q (psi)	t (mm)	t (in)	s_o (mm/mm)	F_1	F_2	Hz	P_N
20.68	3	22.16	3.21	1.465	0.213	1.471	0.213	0.0254	0.001	0.00055	14.70	14.3	4820	3.5
34.47	5	38.51	5.59	3.995	0.579	4.037	0.586	0.0254	0.001	0.00022	59.57	22.4	7550	1.2
48.26	7	56.09	8.14	7.687	1.115	7.829	1.136	0.0254	0.001	0.00047	126.12	30.3	10210	0.63
50.33	7.3	58.83	8.53	8.337	1.209	8.503	1.233	0.0254	0.001	0.00051	137.92	31.6	10650	0.58
55.16	8	65.34	9.48	9.950	1.443	10.18	1.476	0.0381	0.0015	0.00035	42.22	19.8	9990	0.73
68.95	10	84.71	12.29	15.27	2.215	15.77	2.287	0.0381	0.0015	0.00060	71.32	24.0	12140	0.47
103.4	15	138.3	20.05	32.90	4.772	34.83	5.052	0.0762	0.003	0.00041	12.28	13.9	14060	0.43
137.9	20	198.9	28.84	56.11	8.139	60.97	8.843	0.1016	0.004	0.00038	6.42	12.2	16450	0.32
172.4	25	266.3	38.62	84.25	12.219	93.92	13.622	0.1016	0.004	0.00092	15.45	14.6	19700	0.21
206.8	30	340.3	49.35	116.8	16.934	133.4	19.351	0.1422	0.0056	0.00036	3.06	11.3	21300	0.21
241.3	35	420.5	60.99	153.2	22.213	179.2	25.989	0.1422	0.0056	0.00089	7.63	12.6	23800	0.15
275.8	40	506.7	73.50	193.0	27.997	230.9	33.496	0.1803	0.0071	0.00020	1.06	10.5	25130	0.15
310.3	45	598.7	86.83	236.0	34.236	288.4	41.834	0.1803	0.0071	0.00073	3.88	11.5	27500	0.12
344.7	50	696.1	100.96	281.9	40.884	351.4	50.963	0.1803	0.0071	0.00131	6.97	12.3	29440	0.10

Figure 7 shows a plot of F_2 versus F_1 ; where:

$$\begin{aligned} F_1 &= 12 R^2 s_o (1 - \sigma^2)/t^2 \\ F_2 &= 2 R^2 \omega_m \sqrt{3 \rho_d (1 - \sigma^2)}/(t \sqrt{Eg}) \end{aligned} \quad (14)$$

where:

ω_m = mechanical fundamental frequency of diaphragm, radians/second

g = acceleration due to gravity

ρ_d = density of diaphragm material (8000 kg/m³ or 0.289 lbf/in³).

To obtain the fundamental frequency F_1 is calculated, and F_2 is read from the curve in Figure 7. Then from Equation 14:

$$\omega_m = F_2 t \sqrt{Eg} / \left[2 R^2 \sqrt{3 \rho_d (1 - \sigma^2)} \right] \quad (15)$$

and

$$f = t \sqrt{Eg} F_2 / \left[4\pi R^2 \sqrt{3 \rho_d (1 - \sigma^2)} \right] \quad (16)$$

where f is in Hertz.

Values of F_1 , F_2 and f are listed in Table I.

The amount of non-linearity and the magnitude of the fundamental frequency seem adequate for gages to be used on large explosions. The only non-linearity significantly greater than one percent is for the diaphragm used at the lowest pressure listed. This non-linearity can be reduced if the diaphragm sensing technique operates satisfactorily with a peak diaphragm deflection less than 0.01 mm.

The acoustic resonance frequency is difficult to calculate accurately for the proposed gage configuration. Considering the conical stagnation pressure inlet as a closed end tube, a value of about 9000 Hz is obtained for the lowest pressure of interest. The acoustic resonance frequency for the gage may well fall near the fundamental frequency of the diaphragm, and hence the use of acoustical damping may be necessary to avoid undesirable ringing.

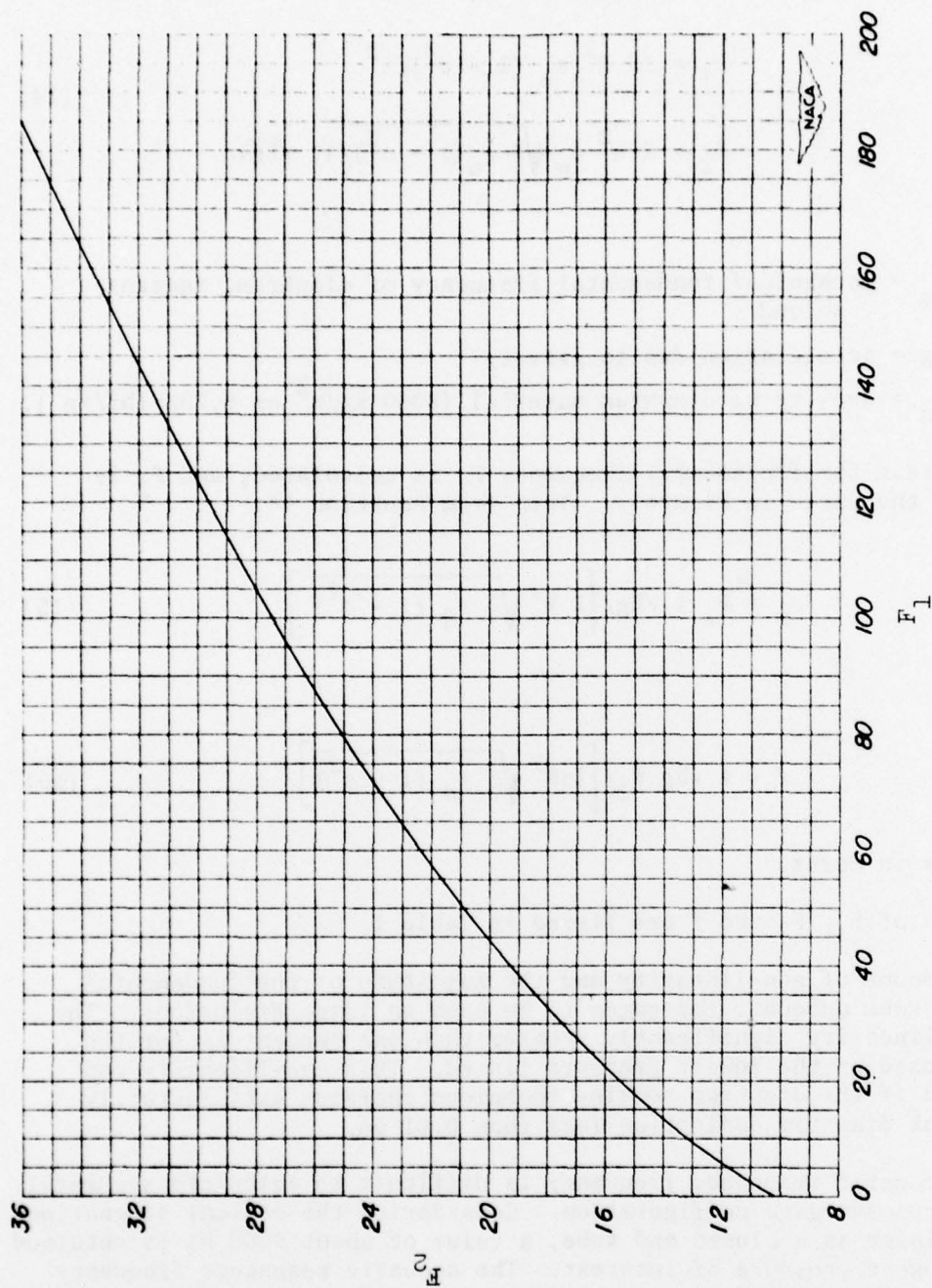


Figure 7 Graphical solution for the fundamental frequency of any clamped, circular, flat diaphragm under radial tension, from Reference 2.

V. SUMMARY

The inadequacy of the current technique for determining dynamic pressure at low incident shock side-on overpressures was demonstrated by presenting the possible error which may occur by use of independent stagnation and side-on overpressure measurements with an error of three percent. No substantial reduction in the resulting large error in the dynamic pressure seems possible using this technique.

It was shown that if a single pressure-sensing element can be used to determine the differential pressure between the stagnation and side-on overpressures, then this difference pressure is essentially equal to the dynamic pressure at the lowest side-on overpressures of interest, and that at higher pressures the correction needed is small, so that the error in the dynamic pressure is essentially determined by the error in the differential pressure measurement. The possibility of measuring this pressure with an error no larger than about plus or minus five percent seems reasonable.

A design for a differential pressure gage was developed which seems workable without requiring new technical developments. A particular diaphragm size and material are proposed based on their previous successful use in a family of pressure gages. The design may be further improved for higher frequency response by using smaller diaphragms. However, some experimentation with diaphragm materials and deflection-sensing techniques may be required to achieve a significant reduction in gage size.

The proposed gage, if it performs as expected, will provide measurements of dynamic pressure of satisfactory accuracy in the blast overpressure regime of particular interest for critical items of Army equipment.

ACKNOWLEDGEMENT

The leading edges of the conical stagnation pressure inlet were rounded at the suggestion of Dr. Ray Sedney of the BRL in order to promote smooth flow over the side-on pressure inlet slots.

LIST OF SYMBOLS

e	percent error in P_q
f	fundamental frequency of diaphragm, Hertz
g	acceleration due to gravity, m/s^2
s_o	strain in diaphragm due to initial diaphragm tension, mm/mm
t	diaphragm thickness, mm
u	particle velocity, m/s
w	deflection of diaphragm at center, mm
x	diameter of a static pressure tube, m
x_h	position of taps from base of nose of a static pressure tube, m
x_s	position of taps from center line of stem on a static pressure tube, m
D	diameter of a pressure orifice, mm
D_q	differential pressure, $P_T - P_s$, kPa
E	Young's Modulus of Elasticity, kPa
F_1	function defined in Equation 14 used in solution for fundamental frequency of stretched diaphragm
F_2	function defined in Equation 14 used in solution for fundamental frequency of stretched diaphragm
M	flow Mach number
P_A	ambient atmospheric pressure, kPa
P_N	percent non-linearity of diaphragm deflection
P_q	dynamic pressure, $1/2 \rho u^2$, kPa
P'_q	P_q calculated from Equation 4 using values of P_T and P_s multiplied by 1.03 or 0.97, kPa
P_s	side-on overpressure, kPa

LIST OF SYMBOLS (continued)

P_T	stagnation overpressure, kPa
ΔP_S	magnitude of change in side-on overpressure, kPa
ΔP_T	magnitude of change in stagnation overpressure, kPa
R	diaphragm radius, mm
R_N	ratio of terms in Equation 10 defining non-linearity of diaphragm deflection
γ	ratio of specific heats (assumed to be 1.4)
ρ	air density, kg/m ³
ρ_d	density of diaphragm material, kg/m ³
σ	Poisson's ratio
ω_m	mechanical fundamental frequency of diaphragm, radians/s